



HAL
open science

Axisymmetric Argon-Plasma-Jet Behaviors in Argon Surrounding Based on a Lattice Boltzmann Computational Method

Ridha Djebeli, Bernard Pateyron, Mohammed El Ganaoui, Habib Sammouda

► **To cite this version:**

Ridha Djebeli, Bernard Pateyron, Mohammed El Ganaoui, Habib Sammouda. Axisymmetric Argon-Plasma-Jet Behaviors in Argon Surrounding Based on a Lattice Boltzmann Computational Method. 2008. hal-00424451v1

HAL Id: hal-00424451

<https://hal.science/hal-00424451v1>

Submitted on 15 Oct 2009 (v1), last revised 17 Dec 2010 (v2)

HAL is a multi-disciplinary open access archive for the deposit and dissemination of scientific research documents, whether they are published or not. The documents may come from teaching and research institutions in France or abroad, or from public or private research centers.

L'archive ouverte pluridisciplinaire **HAL**, est destinée au dépôt et à la diffusion de documents scientifiques de niveau recherche, publiés ou non, émanant des établissements d'enseignement et de recherche français ou étrangers, des laboratoires publics ou privés.

Axisymmetric Argon-Plasma-Jet Behaviors in Argon Surrounding Based on a Lattice Boltzmann Computational Method

R. Djebali, B. Pateyron, M. El Ganaoui, H. Sammouda

I. Introduction

The introduction of plasma spray torches was in 1957 by Thermal Dynamic Corp. (Lebanon, NH). Since that, plasma spraying was an attractive option for its use in materials processing, former, for the aeronautics industry, especially NASA, and later for the aircraft industry (resistance to heat, wear, erosion, and/or corrosion treatment) [1]. Plasma jets are used mainly for the spraying, decomposition, and synthesis of new materials. The use of the plasma jet strongly extended the technological possibilities to any material that could melt. The plasma jets produced discharging at pressures close to atmospheric one are characterized by the high temperatures (around 5000-15000 K, far above the melting temperature, and vapor temperature of any known material) of heavy species and high velocities (between 100 m/s and 2500 m/s) of plasma flow. Hence, a complex flows under these conditions.

Numerous experimental and numerical efforts are conducted in this subject to reach high performances (of surfaces treatments and coating), for economic constraints and to well understand the complex heat, momentum and mass transport coupling. This is because plasma temperature and flow fields, in the flow core, affect absolutely the in-flight particles trajectories, and their temperature histories and then the quality and the formability of thermal spray.

Dealing with plasma jet, in one side, as former studies, E. Pfender et al. [2] have performed a simulation of Argon plasma and compared their results to available experimental measurements.

These studies and others ones deal with 3D, 2D, and 2D1/2(axisymmetric), with and without swirling-velocity in both laminar and turbulent regimes [3]-[7]. It has been shown, then, that thermal and dynamic behaviors of plasma jets depend on a great deal of parameters that interacts starting from burner chamber to the coating formation. In this context, P. Fauchais presents in [4] a review on modeling and measurements in plasma spraying process, development of new torches design and the recent researches. M. Vardelle et al. [5] have identified the influence of nine control parameters (such as carrier gas flow rate, injector (internal diameter), powder size distribution, arc current, size of plasma gun nozzle, plasma gas nature, flow rate, and surrounding atmosphere). In a comparative study, D.-Y. Xu et al. [8] have shown that using argon instead of air as surrounding gas of a laminar argon plasma jet avoids undesired oxidation of metallic materials and increases the length of jet high-temperature region and the mass flow rate but decreases the gas specific enthalpy in the jet downstream region.

It is worth noting that argon plasma jet is at the head of plasma gas nature investigated, and that most authors employed a two-dimensional or pseudo-three-dimensional models [9]. Often the $K - \epsilon$ turbulent models are employed [10], however such models introduce large errors (comparatively to DNS and LES turbulence studying) that can be damped into the viscosity as it is noticed in [11]. Some others 3D studies are performed by using a commercial computational fluid dynamics package [12]-[13]. In other side available modeling works are almost all based on the steady flow assumption in a time-averaged sense [9], [10], [12]. However it has been shown in [14] that the plasma jet is unsteady.

In the last decades, the Lattice Boltzmann (LB) method is considered versus classical approaches to solve complex problems of heat and fluid flow [15]-[26]. Its time-dependent scheme is in accordance with unsteady plasma jet nature. In addition, the LB equation is particularly (fundamentally) adopted to simulating gas flows, which present a collisional process.

The present paper is an approach to reach a fully LB-understanding of the underlying physical processes and characteristics in argon plasma jet. It aims also is to enrich the numerical basis in modeling the plasma dynamics.

In the other side, plasma jet refers to one of the most complex flows, namely for its multiphase/ multicomponent character when spraying. This includes interface instability, bubble/droplet dynamics, wetting on solid surfaces, interfacial slip, and droplet electro-hydrodynamic deformations. Simulating these kinds of flows has always been a challenge to conventional CFD because of the moving and deformable interfaces between phases or components originate from the specific interactions among fluid molecules. Therefore it is difficult to implement such microscopic interactions into the macroscopic Navier–Stokes equation. However, in LBM, the particulate kinetics provides a relatively easy way to incorporate the microscopic interactions by modifying the collision operator. As a multiphase/ multicomponent flow, plasma jet and plasma spraying represent a new field for LB simulation and modeling. The computational cost will be reduced effectively for the phase separation. It will be generated automatically from the

particle dynamics and no special treatment is needed to manipulate the interfaces as in traditional CFD methods.

The first intend for simulating plasma jet using LB method was with H. Zhang et al. [26-27] in a 2D symmetric configuration; however plasma jet flows have a axisymmetric character.

In this work we will perform a numerical simulation of plasma jet in an axisymmetric configuration based on the Jian's model [28]. Furthermore, it is well to mention that plasma jet is laminar in its core but turbulent in its fringes due to the high field gradients (200 K/mm and 10 m/s/mm).

In the present paper, the LBM scheme is employed for simulating the turbulent plasma flow in coupling with the mass, momentum and energy conservation equations. For practical reasons we will focus our attention on the Smagorinsky turbulence model.

The paper is organized as follows: The first section is concerned about the numerical model accounting for turbulence and temperature dependent diffusion parameters. Second section deals with a parametric modeling of the axisymmetric configuration. Third section defines the computing procedure. The forth section focuses on the computational results and discussions.

II. Numerical model

II.1. Basic Assumptions

The assumptions used in this study include

- the argon plasma jet is issuing into argon surrounding (i.e. Ar-Ar),
- the plasma jet flow is time-dependent during the computation, axisymmetric and turbulent;
- the plasma is in the Local Thermodynamic Equilibrium (LTE) state and the radiation heat loss is neglected;
- all the plasma properties are temperature dependent;
- the swirling velocity component in the plasma jet can be neglected in comparison with the axial velocity;
- the plasma jet flow is incompressible [27], then obeys to the condition low Mach number, hence the compression work and the viscous dissipation can be neglected in the energy equation,
- the gravity effect is neglected.

II.2. Governing equations

Based on the above-mentioned assumptions, the continuity, momentum and energy equations in (z, r) coordinates are, in tensor form, as follows:

$$\begin{cases} \frac{\partial u_j}{\partial x_j} = -\frac{u_r}{r} \\ \frac{\partial u_i}{\partial t} + u_j \frac{\partial u_i}{\partial x_j} = -\frac{1}{\rho} \frac{\partial p}{\partial x_i} + \nu \frac{\partial^2 u_i}{\partial x_j^2} + \frac{\nu}{r} \frac{\partial u_i}{\partial r} - \frac{\nu u_i}{r^2} \delta_{ir} \\ \frac{\partial \theta}{\partial t} + u_j \frac{\partial \theta}{\partial x_j} = \alpha \frac{\partial^2 \theta}{\partial x_j^2} + \frac{\alpha}{r} \frac{\partial \theta}{\partial r} - \frac{\dot{w}}{\rho C_p} \end{cases} \quad (1)$$

Were t the time, u_r and u_z are the radial and axial velocities respectively, ρ is the density, θ is the gas temperature, ν is the kinetic viscosity, α is the thermal diffusivity, C_p is specific heat at constant pressure, p is the pressure, \dot{w} is the radiation power per unit volume of plasma (ie in W/m^3) and δ_{ir} is the Kronecker delta function defined as:

$$\delta_{ir} = \begin{cases} 0 & \text{if } i \neq r \\ 1 & \text{if } i = r \end{cases} \quad (2)$$

II.3. Thermal lattice Boltzmann method and the axisymmetric formulation for incompressible fluid flows

In general, the current thermal models fall into the categories: the multispeed approach, the internal energy

distribution model and the passive scalar approach. The multispeed approach is not appropriate for this kind of flows [26]. The passive scalar approach is found to be simpler, in implementing the boundary conditions, then the internal energy distribution model. In this study, we will use the passive scalar approach for computing the temperature field. In other side, it is well known that the most employed 2D lattice Boltzmann model is the D2Q9 one, used in square lattice.

We have found that the D2Q9-D2Q4 is a suitable model for simulating thermal flows. First it is more stable then the D2Q9-D2Q9 model. Second, it preserves the computation effort, because the collision step takes around 70% of the CPU time.

The standard lattice Boltzmann method is used is Cartesian coordinates. The first intend to represent axisymmetric flow [30]. However, the temperature field was solved by using Finite Difference method. Recently, some new formulations are available [17, 23, 25, 26-30]. The Jian's model [23] will be used in this work for simplicity.

The proposed LB model can be written, for the nine velocity directions $0 \leq k \leq 8$, as follows:

$$f_k(\mathbf{x} + \Delta\mathbf{x}, t + \Delta t) - f_k(\mathbf{x}, t) = -\frac{1}{\tau_v} [f_k(\mathbf{x}, t) - f_k^{eq}(\mathbf{x}, t)] + \Delta t F_l + \frac{\Delta t}{6} \mathbf{e}_{ki} \mathbf{F}_{2i} \quad (3)$$

Where Δt is lattice time unit, \mathbf{x} is the lattice site, f_k and f_k^{eq} are the density distribution function and its equilibrium part

$f_k^{eq}(\mathbf{x}, t) = \omega_k \rho [1 + 3 \mathbf{e}_k \cdot \mathbf{u} + 4.5 (\mathbf{e}_k \cdot \mathbf{u})^2 - 1.5 \mathbf{u}^2]$, $F_l = -\frac{\rho u_r}{9r}$ is a source term, τ_v is the single relaxation time for the

density distribution function and is linked to the kinetic viscosity as $\nu = \frac{\tau_v - 0.5 \Delta x^2}{3 \Delta t}$,

$\mathbf{F}_{2i} = -\rho \left[\frac{u_i u_r}{r} - \frac{u}{r} \frac{\partial u_i}{\partial r} + \frac{u u_i}{r^2} \right]$ is a force term, ω_k are a factors and \mathbf{e}_k are the lattice velocity vectors. For the D2Q9

model we have: $\omega_0 = 4/9$, $\omega_k = 1/9$ for $k=1,4$ and $\omega_k = 1/36$ for $k=5,8$; $\mathbf{e}_0 = (0,0)$,

$\mathbf{e}_k = (\cos(k-1)\pi/2, \sin(k-1)\pi/2)$ for $k=1,4$ and $\mathbf{e}_k = (\cos((k-5)\pi/2 + \pi/4), \sin((k-5)\pi/2 + \pi/4))$ for $k=5,8$.

Further reading on the model can be found in [23].

The macroscopic variables, density and velocity, can be computed as follows:

$$\rho(\mathbf{x}, t) = \sum_k f_k \quad (4)$$

$$\mathbf{u}(\mathbf{x}, t) = \frac{1}{\rho} \sum_k \mathbf{e}_k f_k \quad (5)$$

For heat transport, the temperature evolution equation in the four-speed (D2Q4) lattice Boltzmann model is given, for $0 \leq k \leq 8$, by [31] as:

$$g_k(\mathbf{x} + \Delta\mathbf{x}, t + \Delta t) - g_k(\mathbf{x}, t) = -\frac{1}{\tau_\alpha} [g_k(\mathbf{x}, t) - g_k^{eq}(\mathbf{x}, t)] + 0.25 \Delta t \frac{\tau_\alpha - 0.5}{\tau_\alpha} S \quad (6)$$

With $S = \frac{\alpha}{r} \frac{\partial T}{\partial r} - \frac{\dot{w}}{\rho C_p}$ is considered as a sink term and can be solved by simple FD scheme, and τ_α be the single

relaxation time for the temperature distribution function defined as: $\alpha = \frac{\tau_\alpha - 0.5 \Delta x^2}{2 \Delta t}$. Similarly the macroscopic temperature can be obtained from the distribution function (see [32]).

$$T = \sum_k g_k + \frac{\Delta t}{2} S \quad (7)$$

For simplicity we will adopt in what follows the transformation $(x,r) \rightarrow (x,y)$, no changes will be introduced by the transformation.

II.4. Incorporating a turbulence model in the lattice Boltzmann method

A common approach of turbulence modeling due to Smagorinsky [38] in which the anisotropic part of the Reynolds stress term (see [26] for more explanation on filtering operation and filtered equations) is modeled as:

$$\mathcal{G}_{ij} - \frac{\mathcal{G}_{kk}}{3} \delta_{ij} = -2\nu_t \bar{S}_{ij} = -2C \Delta^2 |\bar{S}_{ij}| \bar{S}_{ij} \quad (8)$$

In which the isotropic part $\frac{\mathcal{G}_{kk}}{3} \delta_{ij}$ of the Reynolds stress term is indistinguishable from the pressure term, δ_{ij} is the Kronecker symbol, C is a known Smagorinsky constant (usually taken * is LBM model), $\Delta = \Delta x = \Delta y$ is filtering width and $|\bar{S}_{ij}| = \sqrt{2\bar{S}_{ij}\bar{S}_{ij}}$ is the magnitude of the large scale strain rate tensor $\bar{S}_{ij} = \frac{1}{2} \left(\frac{\partial u_i}{\partial x_j} + \frac{\partial u_j}{\partial x_i} \right)$;

In the LBM-LES modeling, the value of the collision relaxation time is locally adjusted so that the viscosity is equal to the sum of the physical and the eddy viscosities (ν and ν_t respectively) as (for D2Q9 model):

$$\nu_{tot} = \frac{\tau_{\nu-tot} - 0.5}{3} = \nu + \nu_t = \nu + C \Delta^2 |\bar{S}_{ij}| \quad (9)$$

Fortunately, the strain rate tensor is directly computed from the second kinetic moment of the non-equilibrium part of the distribution function, without taking recourse to the finite-differencing of the velocity field.

$$\bar{S}_{ij} = -\frac{3}{2} \frac{1}{\Delta t \rho(x,t) \tau_{\nu-tot}} \sum_k \mathbf{e}_{ki} \mathbf{e}_{kj} (f_k - f_k^{eq}) \quad (10)$$

The second order equation solution gives

$$\tau_{\nu-tot} = \tau_{\nu-tot}(x,t) = \left(\tau_\nu + \sqrt{\tau_\nu^2 + \frac{18 C \Delta^2 |Q_{ij}|}{\rho(x,t)}} \right) / 2 \quad (11)$$

where $Q_{ij} = \sum_k \mathbf{e}_{ki} \mathbf{e}_{kj} (f_k - f_k^{eq})$.

Similarly for the thermal field, the relaxation time is readjusted using the new thermal diffusivity as

$$\alpha_{tot} = \frac{\tau_{\alpha-tot} - 0.5}{2} = \alpha + \alpha_t = \alpha + \frac{\nu_t}{Pr_t} \quad (12)$$

Where Pr_t is the so called turbulent Prandtl number, usually taken between 0.3 and 1.

II.5. Strategies for accounting the temperature dependent parameters

As mentioned above, argon plasma jet is a high temperature flow. So that, all the physical quantities (viscosity, diffusivity, specific heat, density, sound speed, power radiation,...) are temperature-dependent. The discrete data of these quantities are coded in T&TWinner by [29] and [39]-[46]. To take into account this behavior, we have to describe the way giving the transformation of the real (physical and Ph - indexed) quantities to its LB values (LB indexed). For the viscosity we have:

$$\nu_{Ph} = \frac{\tau_\alpha - 0.5}{3} \frac{\Delta x^2}{\Delta t} = \nu_{LB} \frac{\Delta x^2}{\Delta t} \quad (13)$$

Where $\Delta x = \frac{L_0}{m}$, L_0 is the characteristic length, m is the nodes number along L_0 , and $\Delta t = \frac{c_s}{C_s} \Delta x$, c_s is the LB sound speed, C_s is the physical sound speed [36].

Then $\nu_{LB} = \nu_{Ph} \frac{\Delta t}{\Delta x^2} = \nu_{Ph} \frac{c_s}{C_s} \frac{m}{L_0}$. Similarly for the diffusivity, we have $\alpha_{LB} = \alpha_{Ph} \frac{\Delta t}{\Delta x^2} = \alpha_{Ph} \frac{c_s}{C_s} \frac{m}{L_0}$.

In our study, the LB viscosity (and the physical diffusivity) is fitted to polynomial curves, compromising the stability condition $\nu_{LB} > 2.5 \cdot 10^{-3}$, so that we have to act on the quantity $\frac{m}{L_0}$. The same procedure is applied to the thermal diffusivity.

For general cases, one obtains the same dimensionless value when making adimensional a quantity ϕ in LB-space and Ph-space as:

$$\frac{\phi_{LB}}{LB_scale} = \frac{\phi_{Ph}}{Ph_scale} \quad (14)$$

Then,

$$\phi_{LB} = \frac{LB_scale}{Ph_scale} \phi_{Ph} \quad (15)$$

The Table 1 summarizes the conversion rules between LB quantities and their corresponding physical values.

III. Model and solution procedure

III.1.1. Model

A half plan is considered as a computational domain for the axisymmetric plasma jet. The graph is mapped in Figure 1. Where $W=12 \cdot R=48$ mm, $L=100$ mm. AB is the anode thickness, then, no-slip boundary ($\mathbf{u}=0$) condition and a fix temperature ($T_{\min}=700\text{K}$) are retained. BC is a fixe temperature ($T_{\min}=700\text{K}$) and free bound for the velocity ($\partial \mathbf{u} / \partial \mathbf{n}=0$) are adopted. CD is a boundary that we will describe later. OD is an axisymmetric boundary (see [25] for further details). OA is governed by the inlet condition of Eq. (14).

$$\begin{cases} u_{in} = u_{\max} \left[1 - \left(\frac{y}{R} \right)^a \right] \\ T_{in} = (T_{\max} - T_{\min}) \left[1 - \left(\frac{y}{R} \right)^b \right] + T_{\min} \end{cases} \quad (16)$$

TABLE I
Conversion between LB quantities and their corresponding physical (real) values

Denomination	LBM context	Physical context
Space step	$\Delta x = 1$	$\Delta x = \frac{L_0}{m}$
Time step	$\Delta t = 1$	$\Delta t = \frac{c_s}{C_s} \Delta x$
Sound speed	$c_s = 1/\sqrt{3}$ for D2Q9	C_s (temperature dependent)
Kinetic viscosity	$\nu_{Ph} = (\tau_\nu - 0.5)c_s^2$	$\nu_{Ph} = \nu_{LB} \frac{C_s}{c_s} \frac{L_0}{m}$
Thermal diffusivity	$\alpha_{Ph} = (\tau_\alpha - 0.5)c_s^2$	$\alpha_{Ph} = \alpha_{LB} \frac{C_s}{c_s} \frac{L_0}{m}$
Velocity	$\mathbf{u}_{LB} = \frac{1}{\rho} \sum_k \mathbf{e}_k f_k$	$\mathbf{u}_{Ph} = \mathbf{u}_{LB} \frac{\nu_{Ph}}{\nu_{LB}} \frac{m}{L_0}$
Temperature	$\theta = \sum_k g_k$	$T = (T_{\max} - T_{\min})\theta + T_{\min}$

Fig.1. Computational domain

Where u_{\max} and T_{\max} are the velocity and temperature of the plasma jet at the torch axis, T_{\min} , the temperature of the anode, set to $700 K$, and R be the jet-radius at the torch exit. The parameters a and b give the forms of the inflow conditions. Table 2 summarizes some used values. It is well remarked the non universal choice of the two parameters. However, [51, 52] assume the values subject to the constraints provided by the given values of argon mass flow rate and net torch power. In our study we will use $a=3$ and $b=4$.

The domain sizes are as follows: $0 \leq x \leq 100 mm$, $0 \leq y \leq 48 mm$. The domain is mapped by a uniform computational mesh.

TABLE II
Some values of inlet profiles parameters (a,b)

(a, b)	Authors
(1.4, 2.3)	[10]-[45]
(2, 2)	[42]-[44]
(2, 4)	[26]-[27]
(4, 4)	[8]-[13]
(3, 9)	[51]
(2, 4.5)	[52]
(∞ , ∞)	<i>Jet&Poudres</i> [33]

III.1.2. Solution procedure

1. Specify the boundary conditions of the plasma jet flow(velocity and temperature),
2. Specify the inlet conditions of the plasma jet (velocity and temperature inlet profiles),
3. Calculate the inlet LB parameters from the real ones,
4. Specify the LB-viscosity and diffusivity (temperature-fitted curves),
5. Predict the plasma flow fields to obtain the flow temperature and velocity distributions,
6. Check the flow state through a node velocity or a node temperature,
7. Calculate the new LB-viscosity and diffusivity and repeat steps 5, 6 and 7 until the regime is established,
8. End.

IV. Results and discussion

Mostly, numerical plasma jet simulations omit work-piece. However, work-piece constitutes a different boundary condition when spraying in spite of the most taken, free boundary. In our study we consider the two cases, with and without work-piece. When taking account of work-piece, the plasma jet shows an appreciable deformation in temperature and velocity field traces when impinging upon the substrate, likes it is shown in [3], [47].

IV.1.1. Validation analysis and beyond for free jet

In this case the CD edge is a free boundary and the classic extrapolation condition is adopted. The computing inlet conditions are $T_{max}=13500$ K and the velocity takes three values: 520m/s which serves for validation with Pfender [2] and *Jet&Poudres* [33] results and 610 m/s and 700 m/s to put on view the inlet velocity effects on plasma jet behavior.

To show the ability of our thermal model to simulation axisymmetric flows, we consider, in figures 2 and 3, the present centerlines velocity and temperature distributions compared to available numerical and measured results [2] and by using the *Jet&Poudres* software [33] (with conditions $u_{max} = 520$ m/s, $T_{max} = 13500$ K, gaz: argon flowing into stagnant argon). The velocity and temperature profiles of our simulation compare well to the numerical and experimental results of Pfender. It is well noticed that the axial temperature gradient near the inlet (interval 0-25 mm) is close to 185 K/mm then close to 200 K/mm observed experimentally (counter 136 K/mm and 152 K/mm for *Jet&Poudres* and Pfender results respectively) and the velocity gradient is close to 10.76 (m/s)/mm (counter 10.48 (m/s)/mm and 9.48 (m/s)/mm for *Jet&Poudres* and Pfender results respectively) which agree well with former experimental and numerical observations as noted here-above.

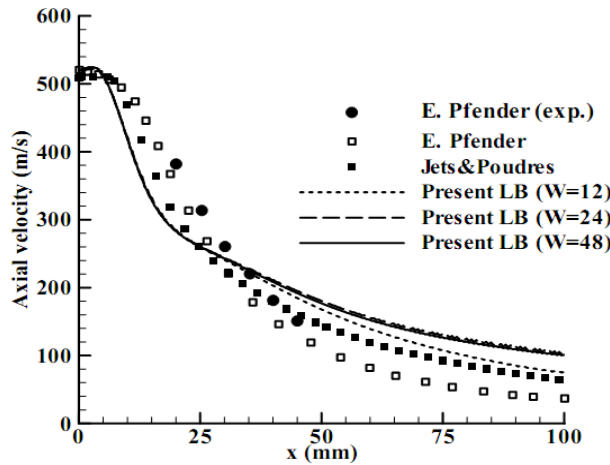


Fig. 2. Centerline-temperature distribution simulated on a LBGK D2Q9 lattice with a Smagorinsky model considering $C_{smag}=0.18$ and $Pr_t=0.3$ in comparison with referenced results.

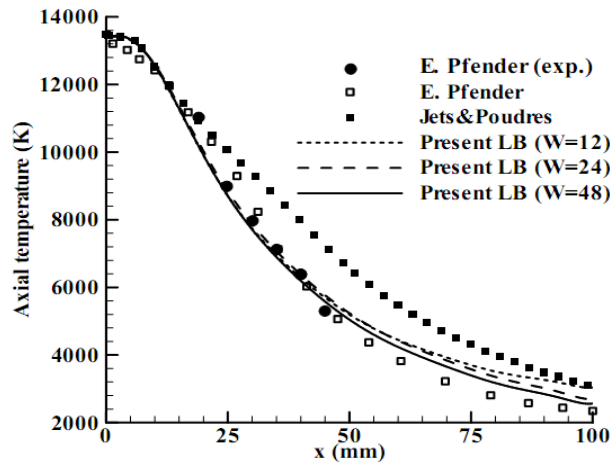


Fig. 3. Centerline-axial velocity distribution simulated on a LBGK D2Q9 lattice with a Smagorinsky model considering $C_{smag}=0.18$ and $Pr_t=0.3$ in comparison with referenced results.

One can also remark that our results go well with *Jet&Poudres* ones. The outlying between the two results in the potential core of the plasma jet (hot zone) is probably due to the fact that ramps are used in *Jet&Poudres* code for the inlet temperature and velocity profiles instead of ours parabolic ones. After that, in the plasma jet core, the profiles become gaussian and the two curves go together.

In the other side, it is clear that the present temperature profile point on the majority of Pfender measured results. For the velocity profile, our LES model seems to be more dissipative than the two other models in the potential core of the plasma jet.

In order to show the efficiency of this approach, it is necessary to conduct some jet analysis, mainly treating the jet width (i), the gaussian temperature and velocity profiles in the jet core region (ii), the effect of computational domain on simulated results (iii), we will take three cases: 12 mm, 24 mm and 48 mm as a mid-width of the domain and finally the effects of maximum inlet velocity on the centerline distribution fields (iv).

Figures 4 and 5 present the isotherms and iso-axial velocities of our results and those of *Jets&Poudres*. It is clear from LB results that the temperature distribution is more expanded then the axial-velocity one, and it shares this characteristic with the Finite-Difference (*Jet&Poudres*) results. In other side, we have extracted the temperature and the velocity values at mid-jet-length and for a jet-width equal to the torch radius, that gives 2298 K and 84 m/s for the LB results counter 4807 K and 75 m/s for *Jet&Poudres* results when the spray distance is 100 mm. For a spray distance of 160 mm we have 1845 K and 72 m/s for LB results counter 3304 K and 56 m/s for *Jet&Poudres* ones. Moreover, one could present the jet width (the jet edge) supposed at $\delta_{0,1}$ as a function of the jet length, where $\delta_{0,1}$ is a characteristic width of the jet expansion at which the velocity becomes 0.1 of its value at the center-line. Figure 6 displays the jet-width as function of the jet-length for both LBGK and *Jets&Poudres* results for the velocity distributions. It is clear that *Jets&Poudres* jet is more expanded and that our results is consistent with the most previous predicted results [3-37-39] where the jet width does not exceed at least 10 mm for the temperature and velocity distributions. This behaviour, for LB results, is in good agreement with experimental plasma-jet characteristics because plasma jet is more extended, however *Jet&Poudres* results are more representative for flame jet which is more expanded.

It might be mentioned that where the teapearture is higher the velocity is higher, then decreasing the probability of evaporating particles when spraying, and similarely when the teapearture is lower, the velocity is lower, then increasing the residence time of flying particles and thus continuing the melt for the solid particles core.

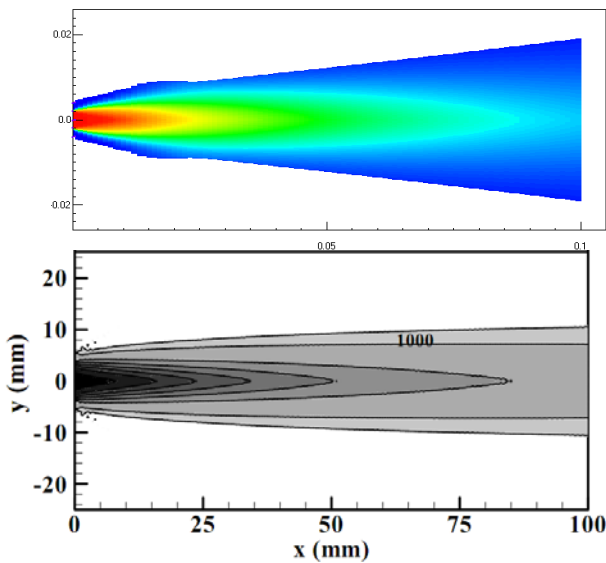


Fig.4. Temperature distributions for *Jet&Poudres* code (above) and LBGK (below) with interval of 2000K and a cutoff color below 750K.

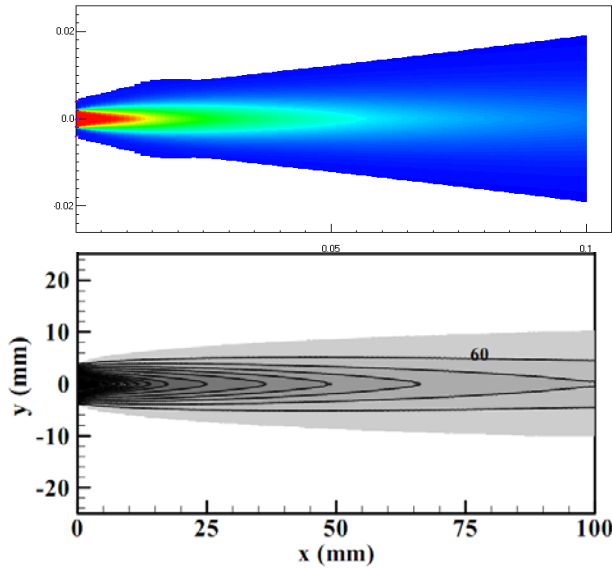


Fig.5. Axial velocity distributions for *Jet&Poudres* code (above) and LBGK (below) with interval of 40m/s and a cutoff color below 20m/s.

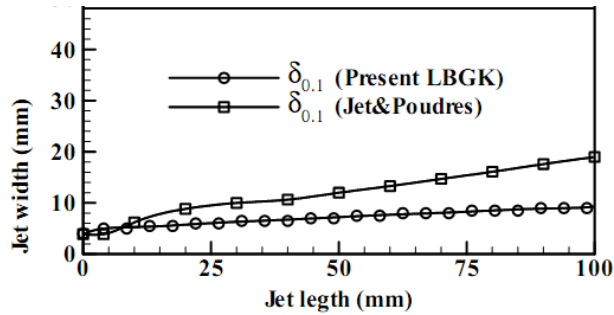


Fig.6. Comparison of the temperature jet edge as function of axial length for *Jet&Poudres* code and the present LBGK.

In simulating and modeling plasma-jets, there is no limitation in the choice of the computational domain, except the typical plasma jet length (spray distance) 100 mm, the plasma jet is observed to be fully developed for about this length. Previous studies are performed for various domain sizes in axial and radial coordinates. In this study we choose to point out the effect of enlarging the computational grille in radial coordinate on the temperature and velocity distributions. Widths 12, 24 and 48 mm are examined here for comparison on the axial distributions. The results are depicted in Figures 2 and 3. It is clear that there is no difference for the three cases until about 40 mm away the nozzle exit, that limited grille influences the distributions of the two fields at the downstream of the jet, and that this influence is minor when the jet width exceeds 24 mm (no big variation between 24 and 48 mm cases).

As we have mention above that the plasma jet has a time dependent character, we note that in our simulations the fluctuations observed, at point (L,0), on a recording process each 5000 times step are between $(76.08 \pm 0.30 \text{m/s}, 3036 \pm 13 \text{K})$, $(103.86 \pm 1.9 \text{m/s}, 3791 \pm 14 \text{K})$ and $(102.13 \pm 1.03 \text{m/s}, 2541 \pm 10 \text{K})$ for the cases $W=12, 24$ and 48 mm respectively.

The velocity vectors traces of our simulation are presented in Figure 7 and are found to match the gaussian distribution radially which prove the free boundary condition taken at the north wall in spite of parabolic profiles shown in [15] which matches the non-slip boundary condition. We, also, may mention that velocity vectors traces give idea about convergence time, in our computations we found that convergence time is reached for about 50 times the number of axial grid.

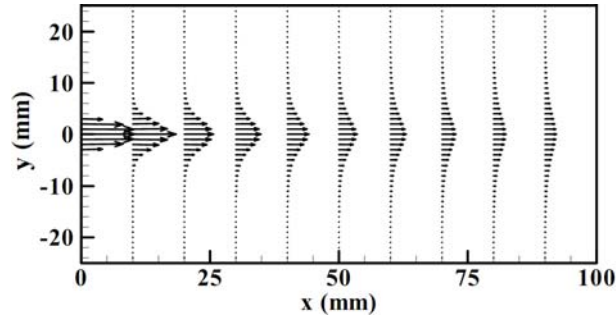


Fig.7. Velocity vectors traces for different cross sections simulated on a LBGK D2Q9 lattice.

Figure 8 shows the radial temperature distributions at different distances from the nozzle exit. The gaussian profile is holds for all the cross sections. The maximum axial temperature decreases with increasing the axial distance, and Gaussian profile becomes more flattened. When dividing by the corresponding axial temperature, we observe that all the curves concur at a radial distance equal to the nozzle radius.

To show the effects of inlet maximum velocity on the centerline temperature and velocity distributions, we perform three computations for values are 520 m/s, 610 m/s and 700 m/s. We have to mention here that plasma jet is, however, incompressible for a Mach number is close to 0.3. For the three inlet velocities the Mach number is 0.217, 0.255 and 0.293 respectively, leading to errors of 4.7%, 6.5% and 8.6% respectively (the accuracy in LB simulations are in order of $O(Ma^2)$). Figure 9 and 10 demonstrate that for high inlet velocity the flow is entertained to the downstream region. For low temperature the fringes translate about 3 mm/(90 m/s) for the thermal field and about 14 mm/(90 m/s) for the dynamic field. One can also say that the axial temperature and velocity gradients near high temperature keep the same above mentioned property when increasing. It is also clear that the outlet temperature increase is of 110 K/(90m/s) and that of the velocity is of 22m/s/(90m/s).

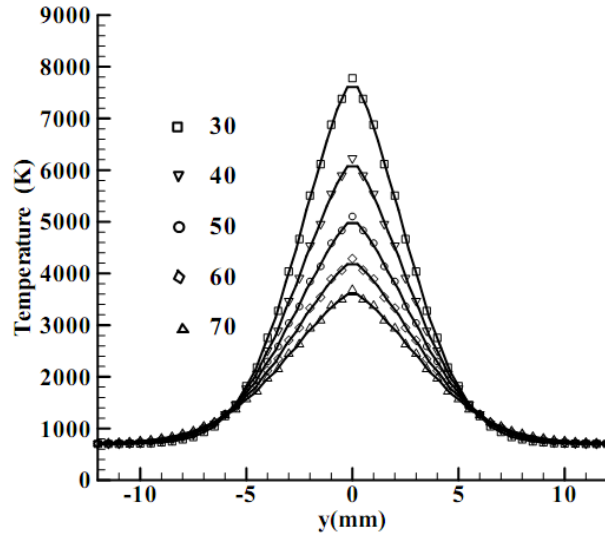


Fig.8. Radial temperature distribution for different cross sections simulated on a LBGK

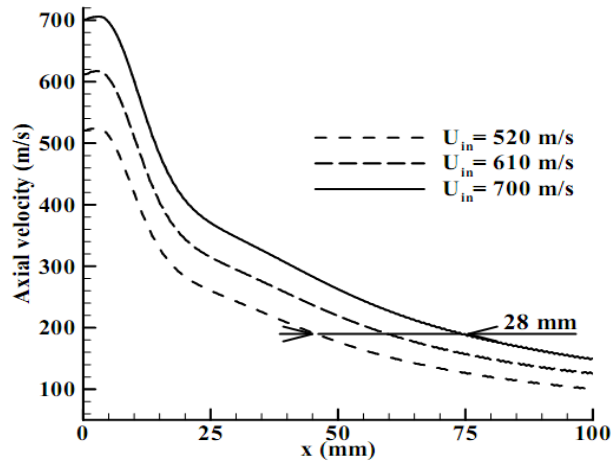


Fig.9. Effect of inlet maximum velocity on centerline-velocity.

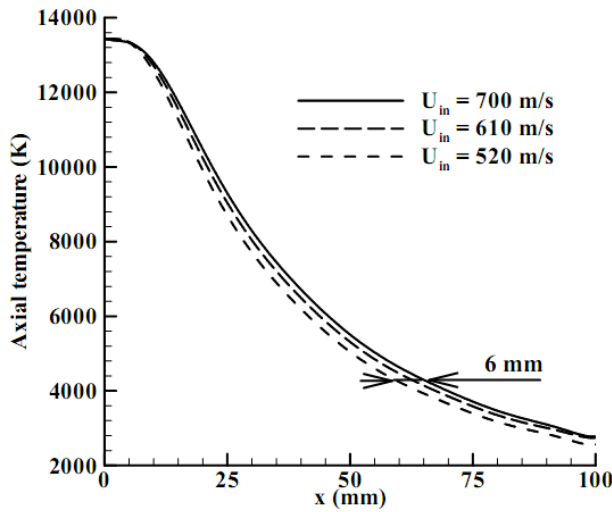


Fig.10. Effect of inlet maximum velocity on centerline-temperature.

IV.1.2. Case with target (substrate)

When spraying, the target, or the substrate, constitutes a new boundary condition for the plasma jet, that is a fix wall boundary in general case. Then it is more intuitive to take in account the derived effects. This behavior have been studied later in [3], [47] and a categorical results have been demonstrated. The temperature and velocity distribution change strongly. The work-piece may have several inclinations with plasma jet axe. We just consider here the case of plasma jet impinging normally on the work-piece. The non-slip boundary condition and low temperature are retained in our treatment. The inlet temperature and velocity are chosen to be 13500 K and 700 m/s, the target stands 100 mm away from the torch exit. Results are depicted in Figures 11 and 12.

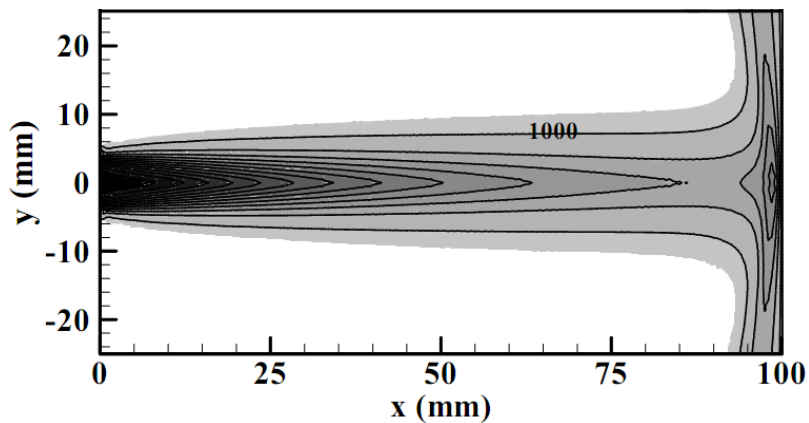


Fig.11. Temperature distribution simulated on a LBGK D2Q9 lattice with a Smagorinsky model considering $C_{smag}=0.18$ and $Pr_t=0.3$ for a jet impinging normally on the substrate with 2000K for the interval and a cutoff color below 750K.

Distributions of figure 11 and 12 are in good agreement with the literature results [3], [47]. The temperature and the axial velocity distributions are flattened locally at the down stream near the work piece. The centerline fields profiles undergo a major variations. The deformation of the jet near work-piece will affect appreciably the sprayed particles trajectories and heating history and particularly its incidence.

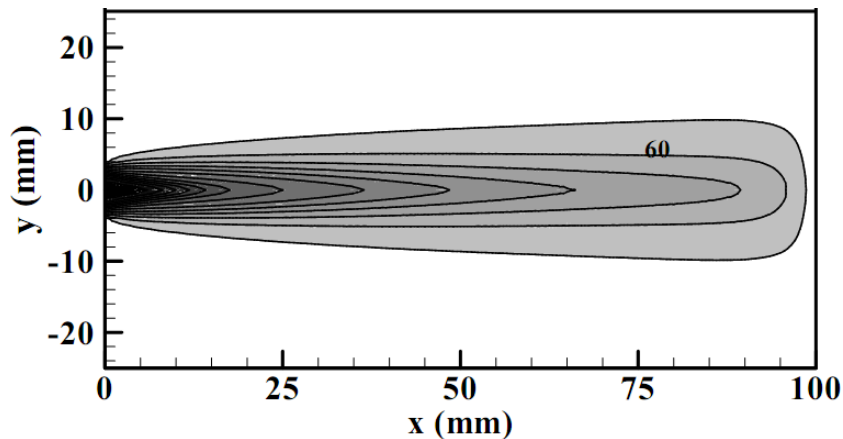


Fig.12. Axial velocity distribution simulated on a LBGK D2Q9 lattice with a Smagorinsky model considering $C_{smag}=0.18$ and $Pr_t=0.3$ for a jet impinging normally on the work-piece with 40m/s for the interval and a cutoff color below 20m/s.

V. Conclusion

In this paper an argon axisymmetric plasma-jet flowing into stagnant argon is simulated by using the Lattice Boltzmann method. The turbulent character is modeled and the temperature dependence of diffusion parameters is taken in account maining to important conclusions dealing with the ability of the approach to simulate complex flows; namely axisymmetric turbulent flows with strong temperature dependent physical parameters. It was shown the possible incorporation of a turbulence model.

The LB method handles easily complex boundary conditions, its linear equation and algebraic operations are more intuitive for overcoming the non linear PDE (Navier-Stokes) in spite of algebraic equations in traditional CFD methods. The time-dependent scheme of the LB equation goes well with the considered unsteady plasma jet character.

The computed centerline temperature and axial velocity by LB method compare well with available numerical and experimental results of previous studies. The temperature and axial velocity distributions are more representative for the axially-extended plasma jet than other available based simulation results.

Increasing the inlet velocity leads to a translation of jet fields to downstream and increases the outlet temperature and axial velocity.

Including the work-piece as a wall boundary affects appreciably the flow structure and changes the field distributions in comparison with the free plasma jet.

The major weak point of our study is, first, to prove the former Navier-stokes predicted results using the lattice Boltzmann method. That is based on the fact that LBM is particularly adopted for gaseous flows, and its scheme is naturally time-dependent. Secondly, to develop a new simple model that serves for this class of complex flows (time-dependent, thermal, free jet, turbulent, temperature dependent viscosity...). Our future works will focus on the study of particle spraying. In this problem, we can treat interacting parameters that influence the dynamic and thermal history of injected particles, such as small/dense particle loading rate, the particles shapes, initial conditions and the account for multiphase and multicomponent flow.

Acknowledgements

We thank CALI and its team, which have allowed the realization of digital simulations to us; CALI is the waiver of calculation of University of Limoges, financed by the area the Limousin, institutes XLIM, IPAM, GEIST, and University of Limoges.

References

- [1] Mariaux, G., Fauchais, P., Vardelle, M., Pateyron, B., Modeling of the plasma spray process : From powder injection to coating formation, *High Temperature Material Processes*, 5 (1), pp. 61-85 (2001)
- [2] E. Pfender, C. H. Chang; Plasma spray jets and plasma-particulates interactions: modeling and experiments; *Proceeding of the 15th International thermal spray conference, 25-29 May 1998, Nice, France.*
- [3] D.-Y. Xu, X.-C. Wu, Xi Chen; Motion and heating of non-spherical particles in a plasma jet; *Surface and Coatings Technology* 171 (2003) 149–156
- [4] P. Fauchais; Understanding plasma spraying: Topical review; *J. Phys. D: Appl. Phys.* 37 (2004) R86–R108
- [5] Ben Ettouil, F., Mazhorova, O., Pateyron, B., Ageorges, H., M. El Ganaoui, M., Fauchais, P., Predicting dynamic and thermal histories of agglomerated particles injected within a d.c. plasma jet, *Surface and Coatings Technology*, 202 (18), pp. 4491-4495, (2008),
- [6] F. Qunbo, W. Lu and W. Fuchi; 3D simulation of the plasma jet in thermal plasma spraying; *Journal of Materials Processing Technology* 166 (2005) 224–229
- [7] H.-B. Xiong , L.-L. Zheng , S. Sampath, R. L. Williamson and J. R. Fincke; Three-dimensional simulation of plasma spray: effects of carrier gas flow and particle injection on plasma jet and entrained particle behavior; *Int. J. Heat and Mass Transfer* 47 (2004) 5189–5200
- [8] D.-Y. Xu and X. Chen; Effects of surrounding gas on the long laminar argon plasma jet characteristics; *International Communications in Heat and Mass Transfer* 32 (2005) 939–946
- [9] H.-P. Li, X. Chen; Three-dimensional simulation of a plasma jet with transverse particle and carrier gas injection; *Thin Solid Films* 390 2001 175-180.
- [10] K. Cheng and X. Chen; Prediction of the entrainment of ambient air into a turbulent argon plasma jet using a turbulence-enhanced combined-diffusion-coefficient method; *International Journal of Heat and Mass Transfer* 47 (2004) 5139–5148.
- [11] A. Dupuis; *From a lattice Boltzmann model to a parallel and reusable implementation of a virtual river*; Univ. Genève, Thesis N°3356 (2002)
- [12] F. Qunbo, W. Lu and W. Fuchi; Modeling influence of basic operation parameters on plasma jet; *journal of materials processing technology* 198 (2008) 207–212
- [13] I. Ahmed and T.L. Bergman; Three-dimensional simulation of thermal plasma spraying of partially molten ceramic agglomerates; *Journal of Thermal Spray Technology*; Volume 9(2) -215; (2000)
- [14] G. Delluc, H. Ageorges, B. Pateyron, P. Fauchais ; Fast modelling of plasma jet and particle behaviours in spray conditions; *High Temp. Mat. Processes*, 9, (2005) 211-226.
- [15] Andrew K. Gunstensen and Daniel H. Rothman; Lattice Boltzmann model of immiscible fluids; *Phys. Rev. A* 43, 4320 - 4327 (1991).
- [16] Xiaowen Shan and Hudong Chen; Lattice Boltzmann model for simulating flows with multiple phases and components; *Phys. Rev. E* 47, 1815 - 1819 (1993).
- [17] S. Succi, E. Foti and F. Higuera; Three-Dimensional Flows in Complex Geometries with the Lattice Boltzmann Method; *Europhys. Lett.* 10 433-438 (1989).
- [18] R. Djebali, M. El Ganaoui, H. Sammouda and R. Bennacer; Some benchmarks of a side wall heated cavity using lattice Boltzmann approach; *FDMP, vol.164, n°1, pp. 1-21, (2009)*
- [19] S. Martys Nicos and Chen Hudong; Simulation of multicomponent fluids in complex three-dimensional geometries by the lattice Boltzmann method; *Physical Review E, Volume 53, Issue 1, pp.743-750, (1996)*
- [20] Xiaowen Shan and Gary Doolen; Multicomponent lattice-Boltzmann model with interparticle interaction; *Journal of Statistical Physics*; vol.81, N°1/2, (1995)
- [21] E. Semma, M. El Ganaoui and R. Bennacer; Lattice Boltzmann method for melting/solidification problems; *C. R. Mécanique*, 335, pp. 295-303. (2007)
- [22] M. Jami, A. Mezrhah, M. Bouzidi and P. Lallemand; Lattice Boltzmann method applied to the laminar natural convection in an enclosure with a heat-generating cylinder conducting body; *Int. J. Thermal Sci.*, 46, pp. 38-47, (2007)
- [23] R. Djebali, M. El Ganaoui and H. Sammouda; Investigation of a side wall heated cavity by using lattice Boltzmann method; *European Journal of Computational Mechanics*, VOL 18/2, pp.217-238, (2009).
- [24] E. Semma, M. El Ganaoui; R. Bennacer and A. A. Mohamad; Investigation of flows in solidification by using the lattice Boltzmann method; *Int. J. Thermal Sci.*, 47, pp. 201-208. (2008).
- [25] Xiaowen Shan and Gary Doolen; Diffusion in a multicomponent lattice Boltzmann equation model; *Phys. Rev. E* 54, 3614 - 3620 (1996).
- [26] H. Zhang, S. Hu and G. Wang and J. Zhu; Modeling and simulation of plasma jet by lattice Boltzmann method; *Applied Mathematical Modelling* 31 1124–1132(2007).
- [27] H. Zhang, S. Hu and G. Wang; Simulation of powder transport in plasma jet via hybrid Lattice Boltzmann method and probabilistic algorithm; *Surface & Coatings Technology* 201 (2006) 886–894.
- [28] J. G. Zhou; Axisymmetric lattice Boltzmann method; *Physical Review E* 78, 036701 (2008).
- [29] B. Pateyron, M.F. Elchinger, G. Delluc and P. Fauchais; Sound velocity in different reacting thermal plasma systems ; *Plasma Chemistry and Plasma Processing*, 16 (1), 39-57, (1996).
- [30] Y. Peng, C. Shu, Y.T. Chew and J. Qiu; Numerical investigation of flows in Czochralski crystal growth by an axisymmetric lattice Boltzmann method; *Journal of Computational Physics* 186 (2003) 295–307.
- [31] S. Mukherjee and J. Abraham; Lattice Boltzmann simulations of two-phase flow with high density ratio in axially symmetric geometry; *Physical Review E* 75, 026701 2007.
- [32] T. Reis and T. N. Phillips; Modified lattice Boltzmann model for axisymmetric flows; *Physical Review E* 75, 056703 2007.
- [33] T. Reis and T. N. Phillips; Numerical validation of a consistent axisymmetric lattice Boltzmann model; *Physical Review E* 77, 026703 2008.
- [34] S. Chen, J. Tölke, S. Geller and M. Krafczyk; Lattice Boltzmann model for incompressible axisymmetric flows; *Physical Review E* 78, 046703,(2008).
- [35] K. N. Premnath and J. Abraham; Lattice Boltzmann model for axisymmetric multiphase flows; *Physical Review E* 71, 056706 2005.

- [36] X. He, S. Chen, G. D. Doolen, (1998): A novel thermal model for the lattice Boltzmann method in incompressible limit, *Journal of Computational Physics*, 146, pp. 282-300.
- [37] D’Orazio A, Corcione M and Celata G P Application to natural convection enclosed flows of a lattice Boltzmann BGK model coupled with a general purpose thermal boundary condition *Int. J. Therm. Sci.* 43 575–86. (2004).
- [38] J. Smagorinsky General circulation experiments with the primitive equations: *I. the basic equations. Mon. Weather Rev.*, 91:99–164, 1963.
- [39] Meillot, E., Vardelle, A., Coudert, J.F., Pateyron, B., Fauchais, P. Plasma spraying using Ar-He-H₂ gas mixtures Proceedings of the International Thermal Spray Conference 1, pp. 803-808 (1998)
- [40] B. Pateyron, G. Delluc and N. Calvé; “T&TWinner”, the chemistry of non-line transport properties in interval 300K to 20000 K, *Mécanique et industries* 6 (6),pp. 651-654, 2005.
- [41] B. Pateyron, G. Delluc and P. Fauchais; Chemical and transport properties of carbon-oxygen hydrogen plasmas in isochoric conditions, *Plasma Chemistry and Plasma Processing*, 25, 485-502, 2005.
- [42] A. Azzou, P. Denoirjean, T. Kameyama, T. Sugiyama, P. Blanchart, Experiments and Model Simulations of the Viscosity and Dilatation of Glass Coatings with Temperature Dependence *J. Am. Ceram. Soc.*, 92 (3) 616-622 (2009)
- [43] Pateyron, B., Elchinger, M.F., Delluc, G., Fauchais, P., Sound velocity in different reacting thermal plasma systems *Plasma Chemistry and Plasma Processing* 16 (1), pp. 39-57 (1996)
- [44] B. Pateyron, *Thèse de doctorat d’Etat*; Université de Limoges (2 Juillet 1987), N° 21-1987; 1987
- [45] B. Pateyron, M.F. Elchinger, G. Delluc and J. Aubreton; *First CODATA Symposium Thermodynamic and thermophysical properties Data base (Paris 3-12 Septembre 1985)*
- [46] “Jets&Poudres” free download from <http://www.unilim.fr/spcts> or <http://jets.poudres.free.fr>
- [47] S. Succi; *The lattice Boltzmann equation for fluid dynamics and beyond*; (book).
- [48] D.-Y. Xu, X. Chen and K. Cheng; Three-dimensional modelling of the characteristics of long laminar plasma jets with lateral injection of carrier gas and particulate matter; *J. Phys. D: Appl. Phys.* 36 (2003) 1583–1594.
- [49] K. Ramachandran, N. Kikukawa and H. Nishiyama; 3D modeling of plasma–particle interactions in a plasma jet under dense loading conditions; *Thin Solid Films* 435 (2003) 298-306.
- [50] K. Cheng, X. Chen and W. Pan; Comparison of Laminar and Turbulent Thermal Plasma Jet Characteristics -A Modeling Study; *Plasma Chem Plasma Process* (2006) 26:211-235.
- [51] C. H. Chang and J. D. Ramshaw; Numerical simulation of nonequilibrium effects in an argon plasma jet; *Phys. Plasmas* 1 (11), November 1994.
- [52] C. H. Chang and J. D. Ramshaw, "Modeling of nonequilibrium effects in a high-velocity nitrogen-hydrogen plasma jet," *Plasma Chem. Plasma Process*, 16, 5S-17S (1996)
- [53] H.-P. Li, X. Chen; Three-dimensional modeling of the turbulent plasma jet impinging upon a flat plate and with transverse particle and carrier-gas injection; *Plasma Chemistry and Plasma Processing*, Vol. 22, No. 1, 2002.